van der Waals epitaxy of CdS thin films on single-crystalline graphene

Xin Sun, Zonghuan Lu, Weiyu Xie, Yiping Wang, Jian Shi, Shengbai Zhang, Morris A. Washington, and Toh-Ming

Citation: Appl. Phys. Lett. 110, 153104 (2017); doi: 10.1063/1.4980088

View online: http://dx.doi.org/10.1063/1.4980088

View Table of Contents: http://aip.scitation.org/toc/apl/110/15

Published by the American Institute of Physics

Articles you may be interested in

Orientation-specific transgranular fracture behavior of CVD-grown monolayer MoS₂ single crystal Applied Physics Letters **110**, 153105 (2017); 10.1063/1.4979974

Carbon nanotube stabilized single layer graphene cantilevers Applied Physics Letters **110**, 151901 (2017); 10.1063/1.4979837

Electronic structure of CdSe-ZnS 2D nanoplatelets Applied Physics Letters **110**, 152103 (2017); 10.1063/1.4980065

Independent tuning of excitonic emission energy and decay time in single semiconductor quantum dots Applied Physics Letters **110**, 151102 (2017); 10.1063/1.4979481

High performance graphene oxide-based humidity sensor integrated on a photonic crystal cavity Applied Physics Letters **110**, 151107 (2017); 10.1063/1.4980045

Decoupling interface effect on the phase stability of CdS thin films by van der Waals heteroepitaxy Applied Physics Letters **110**, 041602 (2017); 10.1063/1.4974855





van der Waals epitaxy of CdS thin films on single-crystalline graphene

Xin Sun,^{1,a)} Zonghuan Lu,¹ Weiyu Xie,¹ Yiping Wang,² Jian Shi,² Shengbai Zhang,¹ Morris A. Washington,¹ and Toh-Ming Lu¹

¹Department of Physics, Applied Physics and Astronomy, and Center for Materials, Devices and Integrated Systems, Rensselaer Polytechnic Institute, Troy, New York 12180, USA

(Received 28 January 2017; accepted 29 March 2017; published online 12 April 2017)

van der Waals epitaxy (vdWE) of three-dimensional CdS thin films on both single-crystalline graphene/Cu(111)/spinel(111) and single-crystalline graphene/SiO₂/Si substrates is achieved via thermal evaporation. X-ray and electron backscatter diffraction pole figures reveal that the CdS films are a Wurtzite structure with a weak epitaxy on graphene and accompanied with a fiber texture background. The epitaxial alignment between CdS and graphene is observed to be an unusual non-parallel epitaxial relationship with a 30° rotation between the unit vectors of CdS and graphene. A geometrical model based on the minimization of superlattice area mismatch is employed to calculate possible interface lattice arrangement. It is found that the 30° rotation between CdS and graphene is indeed the most probable interface epitaxial lattice alignment. The vdWE of CdS on graphene, transferrable to arbitrary substrates, may represent a step forward for the growth of quality CdS thin films on arbitrary substrates through a graphene buffer. *Published by AIP Publishing*. [http://dx.doi.org/10.1063/1.4980088]

van der Waals epitaxy (vdWE) is a concept of locking up substrates and overlayers through the van der Waals force. It was discovered as "physical adsorption with ordering" more than five decades ago and explicitly coined by Koma in 1992.^{1,2} In contrast to chemical epitaxy where a small lattice-mismatch is often an important requirement to grow quality overlayers, vdWE exempts this requirement since chemical bonding does not form at the interface in vdWE. Initially, vdWE did not attract enough attention mainly because the choice of materials for vdWE was limited to a few transition metal dichalcogenides, graphite, mica, and surface-terminated substrates such as H-Si and S-GaAs. But the level of interest in vdWE has been growing in the past years owing to the rapid development of twodimensional (2D) materials which naturally fit the regime of vdWE.³ vdWE systems involving two-dimensional materials consist of three subgroups, namely, two-dimensional (2D) on three-dimensional (3D), 2D-2D, and 3D-2D. The most wellknown example of 2D-3D vdWE is perhaps the epitaxial growth of graphene on single-crystalline substrates. 4–7 There have been numerous studies in this regard. For 2D-2D vdWE, a hot topic, there are also many reports available.8-14 However, there are fewer reports on 3D-2D vdWE.^{2,15-18} In particular, vdWE of 3D materials on graphene has been shown challenging. To date, noteworthy studies regarding vdWE of 3D on graphene include GaN thin films, CdTe thin films, GaAs thin films, GaN nanowires, InAs nanowires, Ge nanocrawlers, SnTe monolayers, and ZnO monolayers. 19-26 Planar films, compared to clusters, are even more challenging to epitaxially grow on graphene, because a typical 3D material would not "wet" the graphene surface. Sometimes, steps or defects have to be created in graphene to promote the nucleation of overlayers. 19,27–29

CdS is a technologically important semiconductor with a host of applications, including photovoltaics, light emitting diode, photodetector, laser, and anti-Stokes cooling. 30-34 While having been explored on mica, 35-37 MoS₂, 17 InSe, 38 and MoTe₂, ¹⁶ vdWE of CdS thin films on graphene has not been demonstrated. Given its extraordinary electronic properties, optical transparency, and transferability to arbitrary substrates, graphene appears to be an attractive choice as the electrode material for CdS-based optoelectronic devices such as CdS/CdTe thin film solar cells. Currently, transparent conductive oxide (TCO) is in place for this role, but semiconductors cannot be grown in single-crystalline form on TCO. Thus, it would be highly desirable if CdS thin film epitaxy can be achieved on graphene that buffers TCO. Note that Seo et al. have fabricated the heterojunction of CdS-graphene by chemical bath deposition, but there was no evidence of epitaxy for that system.²⁷ In this work, we investigate the CdS thin film thermally evaporated on a singlecrystalline graphene transferred to a SiO₂/Si (SOS) substrate. The crystallographic study using electron backscatter diffraction (EBSD) shows signs of epitaxy for the CdS thin film grown on the single-crystalline graphene. To reveal the crystal orientation relationship between CdS and graphene, we also grow an epitaxial CdS film on a graphene/Cu(111)/ spinel(111) surface. The X-ray pole figure of this CdS/ graphene/Cu(111)/spinel(111) sample is used to determine the crystal alignment between CdS and Cu and then correlate CdS with graphene since the graphene is known to be parallelly aligned with Cu(111). Additionally, we use a model based on the minimization of superlattice area mismatch to predict the experimentally observed interface alignment. Both the experiment and the simulation suggest a 30° rotation between CdS and graphene.

110, 153104-1

²Department of Materials Science and Engineering, Rensselaer Polytechnic Institute, Troy, New York 12180, USA

^{a)}Author to whom correspondence should be addressed. Electronic mail: sunx12@rpi.edu

The graphene used in this study was synthesized on a single-crystalline Cu(111) film via a low pressure chemical vapor deposition (CVD) process and then transferred to a SiO₂/Si substrate. Fig. S1 (supplementary material) shows the optical images and Raman spectra of this pre- and posttransferred graphene. While not monolayer everywhere, the graphene is single-crystalline.^{39,40} Fig. 1(a) schematically shows the configuration of a CdS thin film grown on a graphene/SiO₂/Si substrate (GSOS). Since the SiO₂/Si wafer is larger in area than the transferred graphene, we have a control film of CdS on SiO₂/Si (SOS) in the area that is not covered with graphene. The X-ray diffraction (XRD) θ -2 θ scans of these samples are exhibited in Fig. 1(b). The pattern for CdS-SOS shows a wurtzite phase CdS (space group 186) with dominating (0001) orientation, along with a small yet noticeable (10 $\overline{1}$ 3) peak. The peak at \sim 33° is a diffraction from Si. For CdS-GSOS, the out-of-plane orientation is purely wurtzite (0001) or zinc-blende (111). Note that the phase for this CdS is not discriminable without additional peaks, but we have it identified as wurtzite with EBSD. Fig. 1(c) shows the scanning electron microscopy (SEM) image of CdS films spotting at the boundary separating graphene-covered and grapheneuncovered areas. The morphologies of CdS films are sharply contrasted in two areas. Zoom-in SEM images of CdS on GSOS (Fig. 1(d)) and SOS (Fig. 1(e)) show that CdS forms into larger grains when growing directly on the SOS surface than on the graphene buffered surface. To better understand why, cross section SEM images are shown in Fig. S2 (supplementary material), where a striking difference in film thickness can be seen. The CdS film grows much thinner on the GSOS (\sim 330 nm) than that does on the SOS (\sim 1800 nm) after the identical deposition process, suggesting that initially the CdS has difficulty to nucleate on the graphene surface but eventually overcomes it. This also explains the difference in grain size seen in Figs. 1(d) and 1(e). The smaller CdS grains on the GSOS are simply due to the growth of CdS on graphene falling behind at the beginning. It should be mentioned that the CdS film does not grow on the graphene at all after a typical deposition (50 min), whereas it does on the SiO₂/Si substrates. To get the CdS growing on graphene, the deposition has to be extended to 2.5 h in this work, suggesting that the nucleation of CdS on graphene is challenging. All these evidences appear to confirm that the low energy graphene surface is hard to "wet."

Figs. 1(f) and 1(g) show the EBSD crystallographic orientation map $(25 \times 25 \,\mu\text{m})$ and inverse pole figure (IPF) of the CdS-GSOS along sample's Z direction, respectively. The color indexing is shown in the inset of Fig. 1(f). The out-ofplane orientation for this film is $\langle 001 \rangle$, consistent with the XRD data. For the in-plane orientation, Figs. S3(a) and S3(b) (supplementary material) show the EBSD crystallographic orientation maps and IPF of the CdS-GSOS along sample's X and Y directions, respectively. Both X and Y directions of this film are mixed with $\langle 010 \rangle$ and $\langle 120 \rangle$, with the former being preferred along X and the latter along Y. Note that the index translates to $\langle \overline{1}2\overline{1}0 \rangle$ and $\langle 01\overline{1}0 \rangle$ if the four-digit Miller index is used. This means that the in-plane orientation of this CdS film has preferences although is not perfectly aligned. Fig. 1(h) shows the CdS $\{10\overline{1}1\}$ EBSD pole figure for CdS-GSOS. Interestingly, the pole figure is a combination of a ring and six-fold symmetrical poles at the same polar angle ($\chi = 62^{\circ}$). This implies that the microstructure of this CdS film is in between fiber and singlecrystalline texture. Therefore, we can conclude that the CdS film indeed can achieve epitaxy on graphene although weak in the present work. On the other hand, the out-of-plane orientation for CdS-SOS is also $\langle 001 \rangle$, as evidenced by the EBSD crystallographic orientation map $(25 \times 25 \,\mu\text{m})$ and IPF along sample's Z direction in Figs. 1(i) and 1(j), respectively. However, the in-plane orientation for this film is completely random (Figs. S3(c) and S3(d) (supplementary material)). Fig. 1(k) shows the CdS $\{10\overline{1}1\}$ EBSD pole figure for CdS-SOS, where a ring can be found at $\chi = 62^{\circ}$. This indicates a pure fiber structure in this film, which is as expected considering the amorphous nature in the substrate.

Due to the absence of covalent bonding, one may expect to see a strain-free, incommensurate, and random overlayergraphene alignment at the interfaces in vdWE. However, it

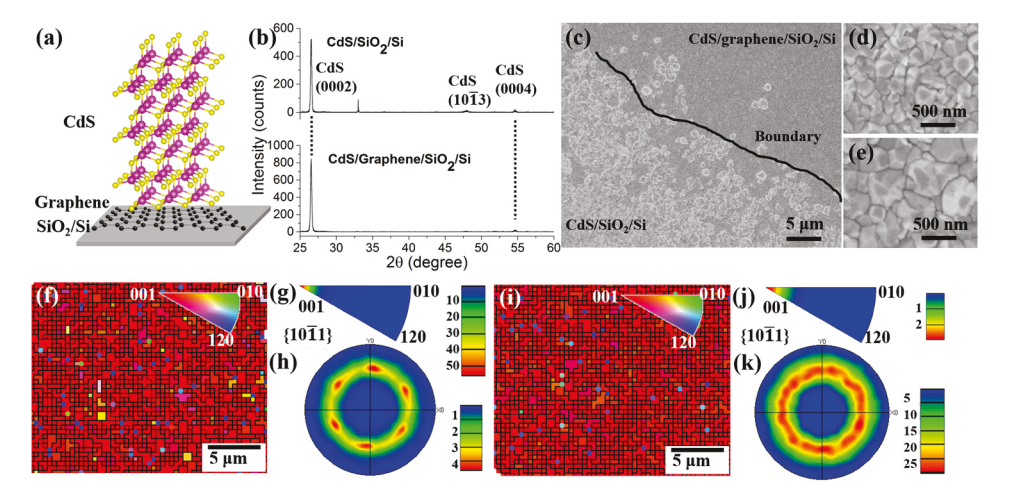


FIG. 1. (a) A Schematic of the 3D CdS film grown on a graphene/SiO₂/Si substrate. (b) XRD $\theta/2\theta$ scans of the CdS films on the graphene/SiO₂/Si and SiO₂/Si substrates. (c) Low magnification SEM image of CdS films spotting at the boundary separating graphene-covered and graphene-uncovered areas. (d) and (e) High magnification SEM images of the CdS film grown on (d) the graphene/SiO₂/Si substrate and (e) the SiO₂/Si substrate. (f)—(h) EBSD crystallographic orientation mapping-Z (f), IPF-Z (g), and CdS { $10\overline{1}1$ } pole figure (h) of the CdS grown on the graphene/SiO₂/Si substrate. (i)—(k) EBSD crystallographic orientation mapping-Z (j), IPF-Z (j), and CdS { $10\overline{1}1$ } pole figure (k) of the CdS grown on the SiO₂/Si substrate.

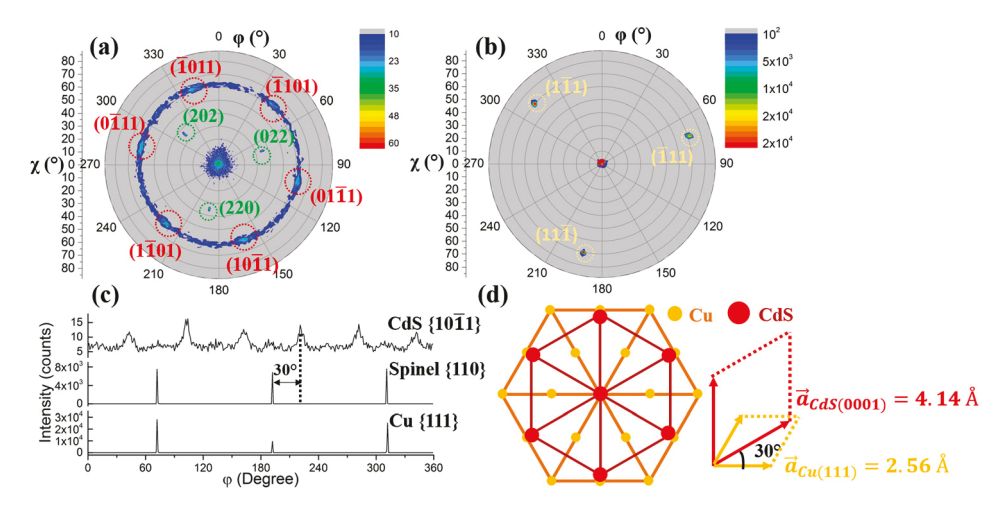


FIG. 2. (a) CdS $\{10\overline{1}1\}$ X-ray pole figure of the CdS film grown on the graphene/Cu(111)/spinel(111) substrate; red: CdS poles; green: spinel poles. (b) Cu $\{111\}$ X-ray pole figure of the CdS/graphene/Cu(111)/spinel(111) sample. (c) Azimuthal (φ) scans of the three poles from CdS, spinel, and Cu. The scan for CdS is an average of ten scans to reduce the noise. (d) 2D lattice overlay for CdS(0001) with respect to Cu(111) deduced from the pole figures and φ scans and the definition of CdS(0001) and Cu(111) 2D unit cells.

has been shown that although it is weak, the vdWE interaction can still induce an in-plane orientation alignment.^{20,41} To determine the relative orientation between CdS and graphene, we perform a parallel study on the epitaxial growth of CdS on a graphene/Cu(111)/spinel(111) substrate. Fig. 2(a) shows the CdS $\{10\overline{1}1\}$ X-ray pole figure, where again a ring and six-fold symmetrical poles can be found at $\gamma = 62^{\circ}$. This suggests that the CdS film grown on the pre-transferred graphene has also a weak epitaxy, similar to that on the posttransferred graphene. The inner three-fold poles at $\gamma = 35^{\circ}$ are attributed to the spinel substrate due to the fact that the spinel {220} Bragg angle is 31.2° and is close to that for CdS $\{10\overline{1}1\}\ (2\theta = 28.4^{\circ})$. Fig. 2(b) shows the Cu $\{111\}$ X-ray pole figure with three-fold poles at $\chi = 70^{\circ}$. The azimuthal (φ) scans for the three sets of poles are plotted in Fig. 2(c), which deduces the alignment of CdS, Cu, and spinel as follows: CdS(0001)||Cu(111)||spinel(111) and CdS $[01\overline{1}0]$ | Cu $[\overline{1}10]$ | spinel $[\overline{1}10]$. This alignment leads to such an interface lattice overlay of CdS(0001) and Cu(111) as shown in Fig. 2(d). Note that the Cu(111) plane can be regarded as a 2D hexagonal lattice. The 2D unit cells for CdS(0001) and Cu(111) are defined in Fig. 2(d). One can see that there is a 30° rotation between $\vec{a}_{CdS(0001)}$ and $\vec{a}_{Cu(111)}$. Considering that graphene $(\vec{a}_{graphene} = \vec{b}_{graphene} = 2.46 \,\text{Å}$ and $\alpha = 60^{\circ}$) is known to be parallelly aligned on Cu(111), 40,42 that is, $\vec{a}_{Cu(111)}||\vec{a}_{graphene}|$, we arrive at the conclusion that $\vec{a}_{CdS(0001)}$ is rotated 30° with respect to $\vec{a}_{graphene}$.

To understand the observed orientation alignment between CdS and graphene, we consider a geometrical superlattice matching model.⁴³ Briefly, when two lattices form heteroepitaxy, they always have many pairs of superlattices close or even identical to each other (coincidence lattices).^{43–45} Physically, it is desirable to have a small

superlattice area since the coincidence superlattice matching density would be high. It is also desirable to have a small difference between the two superlattices for the consideration of the minimization for the system's energy. To incorporate these two considerations, a parameter called superlattice area mismatch, ΔA , is defined as follows:

$$\Delta A = A[(\Delta u/u) + (\Delta v/v) + (\Delta \alpha/\tan \alpha)]. \tag{1}$$

Here, we define the sides (2D lattice) of substrate superlattice as u_1 and v_1 with an angle α_1 between them and overlayer superlattice as u_2 and v_2 with an angle α_2 between them. The superlattice mismatch is defined as $\Delta u \equiv u_2 - u_1$, $\Delta v \equiv v_2 - v_1$, and $\Delta \alpha \equiv \alpha_2 - \alpha_1$. A_1 and A_2 are the superlattice areas of the substrate and overlayer, respectively. For small superlattice mismatches, we have $u_2 \approx u_1 = u$, $v_2 \approx$ $v_1 = v$, $\alpha_2 \approx \alpha_1 = \alpha$, and $A_2 \approx A_1 = A$. In Eq. (1), ΔA can be regarded as a multiplication of two terms: the first is A, which is inversely proportional to the coincidence superlattice matching density; the second is the quantity inside the brackets, which is proportional to the mismatch. Apparently, both terms need be small to form a desirable interface. Then, a small value of ΔA can be obtained and will represent a high chance of the superlattice being observed. With this methodology, Fig. 3(a) shows the calculated result of all possible ΔA (those larger than 25 Å^2 are ignored) using lattice constants of $\vec{a}_{graphene} = 2.46 \,\text{Å}$ and $\vec{a}_{CdS(0001)} = 4.14 \,\text{Å}$. The rotation angle γ is defined as the angle between $\vec{a}_{graphene}$ and $\vec{a}_{CdS(0001)}$. The maximums of A, $\Delta u/u$, $\Delta v/v$, and $\Delta \alpha/\tan \alpha$ are set to be $200 \,\text{Å}^2$, 3%, 3%, and 3%, respectively. The radius of the circles in Fig. 3(a) is scaled inversely proportional to A. In this plot, we can identify that the smallest ΔA (0.88 Å^2) happens to be the data point at $\gamma = 30^\circ$ with the

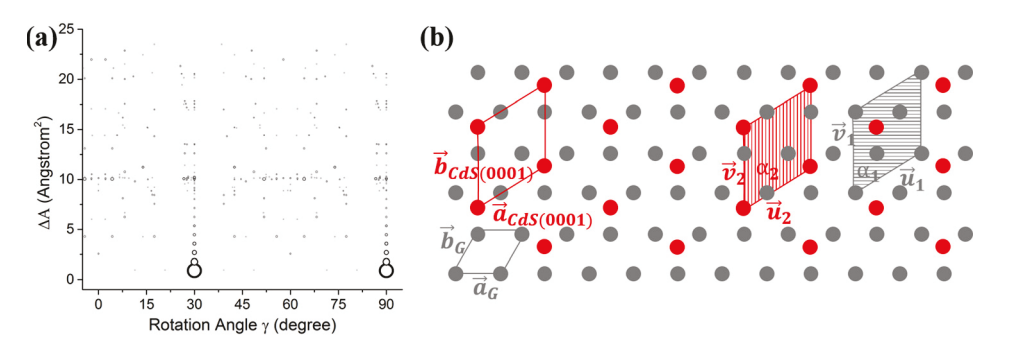


FIG. 3. (a) Superlattice area mismatch (ΔA) plot for CdS(0001) on graphene. The rotation angle γ is defined as the angle between $\vec{a}_{graphene}$ and $\vec{a}_{CdS(0001)}$. (b) 2D lattice overlay for CdS(0001) on graphene when the γ is 30°, which is the most favorable configuration predicted by the ΔA calculation. The unit cells and superlattice cells are labeled in gray and red for graphene and CdS(0001), respectively.

FIG. 4. (a) Raman spectra of the CdS films on the graphene/SiO $_2$ /Si and SiO $_2$ /Si substrates. The full-width-at-half-maximum (FWHM) of 1LO is 12.3 ± 0.4 and 14.1 ± 1.7 cm $^{-1}$, respectively. (b) PL spectra of the CdS films on the graphene/SiO $_2$ /Si and SiO $_2$ /Si substrates. (c) TRPL decay curves of the CdS films on the graphene/SiO $_2$ /Si and SiO $_2$ /Si and SiO $_2$ /Si substrates. The measured carrier lifetime from the former is estimated to be 58 ps on the surface and 324 ps in the bulk, whereas the carrier lifetime from the latter is estimated to be 51 ps and 295 ps for the surface and the bulk, respectively.

largest circle. The result of this calculation is consistent with that observed experimentally. Note that the data point at 90° in γ is equivalent to 30° due to symmetry. Fig. 3(b) shows the 2D lattice overlay of the most favorable alignment of CdS(0001) on graphene. The unit cells of graphene and CdS(0001) are shown in gray and red with $\gamma=30^\circ$. The superlattice parallelograms of graphene and CdS(0001) ($A_1=15.72~\text{Å}^2,~\vec{u}_1=4.26~\text{Å},~\vec{v}_1=4.26~\text{Å},~\alpha_1=60^\circ$ and $A_2=14.84~\text{Å}^2,~\vec{u}_2=4.14~\text{Å},~\vec{v}_2=4.14~\text{Å},~\alpha_2=60^\circ$) are also highlighted, respectively.

Fig. 4(a) shows the Raman spectra of CdS films on GSOS and SOS. The longitudinal optical (LO) phonon mode of CdS up to the 3rd order can be observed in CdS-GSOS, while only the first two LOs in CdS-SOS. The peak positions for these two samples are nearly the same, but the peaks of CdS-GSOS are narrower than those of CdS-SOS. Fig. 4(b) shows the room temperature photoluminescence (PL) spectra. Similar to Raman, the primary PL emission is located at the same position (~505 nm) for both CdS films, and the peak of CdS-GSOS seems a little bit narrower. The main difference between these two is the presence of a shoulder peak (\sim 540 nm) and a tiny red emission (\sim 620 nm) for CdS-SOS. While the origin of the former is unknown yet, the surface state defect is believed to be responsible for the latter. 46 The Huang-Rhys parameter, S, can be calculated to estimate the strength of the exciton-phonon coupling⁴⁷

$$S = 2 \left| \frac{I_{2LO}}{I_{LO}} \right| \frac{(E_{ex} + 2\hbar\omega_{LO} - \hbar\omega_0)^2 + \Gamma^2}{(E_{ex} + \hbar\omega_{LO} - \hbar\omega_0)^2 + \Gamma^2}.$$
 (2)

Here, I is the integrated intensity of the Raman peak, E_{ex} the electronic transition energy, ω_{LO} the frequency of LO phonon, ω_0 the frequency of incident photon, and Γ the linewidth of PL (0.134 eV). For CdS, the free exciton binding energy is 30 meV,⁴⁸ and the bandgap of CdS is 2.45 eV in this work, then E_{ex} can be estimated to be 2.42 eV. The S for CdS-GSOS and CdS-SOS is found to be 1.6 and 1.7, respectively, close to those of similar semiconductors reported in the literature. ^{47,49} Time-resolved PL decay curves can be found in Fig. 4(c). Again, a slightly larger carrier lifetime is found for CdS-GSOS. We believe that all these improvements in terms of optical characterization can be attributed to the better crystal quality of CdS-GSOS over CdS-SOS although the improvement is not significant due to the weakness of epitaxy.

In summary, vdWE of CdS thin films on a singlecrystalline graphene is observed experimentally. While the epitaxy is weak and mixed with a fiber texture, this study confirms the feasibility of growing single-crystalline CdS thin film on graphene. This demonstration could potentially be an upgrade for CdS/CdTe thin film photovoltaics where single-crystalline semiconductor cannot be grown on TCO substrates. We also reveal that the CdS is rotated 30° with respect to graphene in this vdWE, a conclusion supported by both experiments and calculation based on a geometrical superlattice matching model.

See supplementary material for details of experiments, optical images and Raman spectra of graphene, and EBSD results.

This work was supported by the NYSTAR Focus Center at RPI, C130117 and by NSF Awards under CMMI 1550941, CMMI 1635520, and DMR 1305293. The authors would like to thank the Micro and Nano Fabrication Clean Room (MNCR) staff at RPI for facilitating the experimental work.

¹J. G. Dash, Films on Solid Surfaces: The Physics and Chemistry of Physical Adsorption (Academic Press, New York, 1975).

²A. Koma, Thin Solid Films **216**(1), 72 (1992).

³M. I. Bakti Utama, Q. Zhang, J. Zhang, Y. Yuan, F. J. Belarre, J. Arbiol, and Q. Xiong, Nanoscale 5(9), 3570 (2013).

⁴H. Wang, X. Xu, J. Li, L. Lin, L. Sun, X. Sun, S. Zhao, C. Tan, C. Chen, W. Dang, H. Ren, J. Zhang, B. Deng, A. L. Koh, L. Liao, N. Kang, Y. Chen, H. Xu, F. Ding, K. Liu, H. Peng, and Z. Liu, Adv. Mater. **28**(40), 8968 (2016).

⁵J.-H. Lee, E. K. Lee, W.-J. Joo, Y. Jang, B.-S. Kim, J. Y. Lim, S.-H. Choi, S. J. Ahn, J. R. Ahn, M.-H. Park, C.-W. Yang, B. L. Choi, S.-W. Hwang, and D. Whang, Science 344(6181), 286 (2014).

⁶J. Hwang, M. Kim, D. Campbell, H. A. Alsalman, J. Y. Kwak, S. Shivaraman, A. R. Woll, A. K. Singh, R. G. Hennig, S. Gorantla, M. H. Rümmeli, and M. G. Spencer, ACS Nano 7(1), 385 (2013).

⁷K. V. Emtsev, A. Bostwick, K. Horn, J. Jobst, G. L. Kellogg, L. Ley, J. L. McChesney, T. Ohta, S. A. Reshanov, J. Rohrl, E. Rotenberg, A. K. Schmid, D. Waldmann, H. B. Weber, and T. Seyller, Nat. Mater. 8(3), 203–207 (2009).

⁸Q. Ji, Y. Zhang, T. Gao, Y. Zhang, D. Ma, M. Liu, Y. Chen, X. Qiao, P.-H. Tan, M. Kan, J. Feng, Q. Sun, and Z. Liu, Nano Lett. **13**(8), 3870 (2013)

⁹H. Ago, H. Endo, P. Solís-Fernández, R. Takizawa, Y. Ohta, Y. Fujita, K. Yamamoto, and M. Tsuji, ACS Appl. Mater. Interfaces 7(9), 5265 (2015).

X. Zhang, F. Meng, J. R. Christianson, C. Arroyo-Torres, M. A. Lukowski, D. Liang, J. R. Schmidt, and S. Jin, Nano Lett. 14(6), 3047 (2014)

¹¹Z. Liu, L. Song, S. Zhao, J. Huang, L. Ma, J. Zhang, J. Lou, and P. M. Ajayan, Nano Lett. 11(5), 2032 (2011).

¹²X. Ding, G. Ding, X. Xie, F. Huang, and M. Jiang, Carbon **49**(7), 2522 (2011).

- ¹³J. Ji, X. Song, J. Liu, Z. Yan, C. Huo, S. Zhang, M. Su, L. Liao, W. Wang, Z. Ni, Y. Hao, and H. Zeng, Nat. Commun. 7, 13352 (2016).
- ¹⁴Y. Xiang, F.-W. Guo, T.-M. Lu, and G.-C. Wang, Nanotechnology 27(48), 485703 (2016).
- ¹⁵Y. Wang, Y. Shi, G. Xin, J. Lian, and J. Shi, Cryst. Growth Des. **15**(10), 4741 (2015).
- ¹⁶T. Löher, Y. Tomm, C. Pettenkofer, and W. Jaegermann, Appl. Phys. Lett. 65(5), 555 (1994).
- ¹⁷G. Shimaoka, Thin Solid Films **7**(6), 405 (1971).
- ¹⁸Y. Wang, X. Sun, R. Shivanna, Y. Yang, Z. Chen, Y. Guo, G.-C. Wang, E. Wertz, F. Deschler, Z. Cai, H. Zhou, T.-M. Lu, and J. Shi, Nano Lett. **16**(12), 7974 (2016).
- ¹⁹J. Kim, C. Bayram, H. Park, C.-W. Cheng, C. Dimitrakopoulos, J. A. Ott, K. B. Reuter, S. W. Bedell, and D. K. Sadana, Nat. Commun. 5, 4836 (2014).
- ²⁰D. Mohanty, W. Xie, Y. Wang, Z. Lu, J. Shi, S. Zhang, G.-C. Wang, T.-M. Lu, and I. B. Bhat, Appl. Phys. Lett. **109**(14), 143109 (2016).
- ²¹V. Kumaresan, L. Largeau, A. Madouri, F. Glas, H. Zhang, F. Oehler, A. Cavanna, A. Babichev, L. Travers, N. Gogneau, M. Tchernycheva, and J.-C. Harmand, Nano Lett. 16(8), 4895 (2016).
- ²²Y. J. Hong, W. H. Lee, Y. Wu, R. S. Ruoff, and T. Fukui, Nano Lett. 12(3), 1431 (2012).
- ²³E. Mataev, S. K. Rastogi, A. Madhusudan, J. Bone, N. Lamprinakos, Y. Picard, and T. Cohen-Karni, Nano Lett. 16(8), 5267 (2016).
- ²⁴K. Chang, J. Liu, H. Lin, N. Wang, K. Zhao, A. Zhang, F. Jin, Y. Zhong, X. Hu, W. Duan, Q. Zhang, L. Fu, Q.-K. Xue, X. Chen, and S.-H. Ji, Science 353(6296), 274 (2016).
- ²⁵H.-K. Hong, J. Jo, D. Hwang, J. Lee, N. Y. Kim, S. Son, J. H. Kim, M.-J. Jin, Y. C. Jun, R. Erni, S. K. Kwak, J.-W. Yoo, and Z. Lee, Nano Lett. 17(1), 120–127 (2016).
- ²⁶Y. Alaskar, S. Arafin, D. Wickramaratne, M. A. Zurbuchen, L. He, J. McKay, Q. Lin, M. S. Goorsky, R. K. Lake, and K. L. Wang, Adv. Funct. Mater. 24(42), 6629 (2014).
- ²⁷W.-O. Seo, Y. Jung, J. Kim, D. Kim, and J. Kim, Appl. Phys. Lett. 104(13), 133902 (2014).
- ²⁸Y. Jung, G. Yang, S. Chun, D. Kim, and J. Kim, Appl. Phys. Lett. **103**(23), 231910 (2013).
- ²⁹G. Yang, D. Kim, and J. Kim, Opt. Express **23**(19), A1081 (2015).

- ³⁰S. G. Kumar and K. S. R. K. Rao, Energy Environ. Sci. **7**(1), 45 (2014).
- ³¹O. Hayden, A. B. Greytak, and D. C. Bell, Adv. Mater. 17(6), 701 (2005).
- ³²K. Heo, H. Lee, Y. Park, J. Park, H.-J. Lim, D. Yoon, C. Lee, M. Kim, H. Cheong, J. Park, J. Jian, and S. Hong, J. Mater. Chem. **22**(5), 2173 (2012)
- ³³R. Agarwal, C. J. Barrelet, and C. M. Lieber, Nano Lett. **5**(5), 917 (2005).
- ³⁴J. Zhang, D. Li, R. Chen, and Q. Xiong, Nature **493**(7433), 504 (2013).
- ³⁵S. Simov, Thin Solid Films **15**(1), 79 (1973).
- ³⁶K. L. Chopra and I. H. Khan, Surf. Sci. **6**(1), 33 (1967).
- ³⁷X. Sun, Y. Wang, L. J. Seewald, Z. Chen, J. Shi, M. A. Washington, and T.-M. Lu, Appl. Phys. Lett. **110**(4), 041602 (2017).
- ³⁸T. Löher, A. Klein, E. Schaar-Gabriel, R. Rudolph, Y. Tomm, M. Giersig, C. Pettenkofer, and W. Jaegermann, Van Der Waals Epitaxy of II-Vi Semiconductors on Layered Chalcogenide (0001) Substrates: Towards Buffer Layers for Lattice Mismatched Systems? (Mater. Res. Soc. Symp. Proc., 2011), Vol. 441, pp. 597–601.
- ³⁹Y. Ogawa, B. Hu, C. M. Orofeo, M. Tsuji, K.-I. Ikeda, S. Mizuno, H. Hibino, and H. Ago, J. Phys. Chem. Lett. 3(2), 219 (2012).
- ⁴⁰Z. R. Robinson, P. Tyagi, T. R. Mowll, C. A. Ventrice, and J. B. Hannon, Phys. Rev. B 86(23), 235413 (2012).
- ⁴¹C. R. Woods, L. Britnell, A. Eckmann, R. S. Ma, J. C. Lu, H. M. Guo, X. Lin, G. L. Yu, Y. Cao, R. V. Gorbachev, A. V. Kretinin, J. Park, L. A. Ponomarenko, M. I. Katsnelson, Y. N. Gornostyrev, K. Watanabe, T. Taniguchi, C. Casiraghi, H. J. Gao, A. K. Geim, and K. S. Novoselov, Nat. Phys. 10(6), 451 (2014).
- ⁴²X. Chen, S. Liu, L. Liu, X. Liu, X. Liu, and L. Wang, Appl. Phys. Lett. 100(16), 163106 (2012).
- ⁴³A. S. Yapsir, C. H. Choi, and T. M. Lu, J. Appl. Phys. **67**(2), 796 (1990).
- ⁴⁴A. Zur and T. C. McGill, J. Appl. Phys. **55**(2), 378 (1984).
- ⁴⁵W. Xie, M. Lucking, L. Chen, I. Bhat, G.-C. Wang, T.-M. Lu, and S. Zhang, Cryst. Growth Des. 16(4), 2328 (2016).
- ⁴⁶J. D. Levine and P. Mark, Phys. Rev. **144**(2), 751 (1966).
- ⁴⁷Q. Zhang, J. Zhang, M. I. B. Utama, B. Peng, M. de la Mata, J. Arbiol, and Q. Xiong, Phys. Rev. B 85(8), 085418 (2012).
- ⁴⁸I. Pelant and J. Valenta, *Luminescence Spectroscopy of Semiconductors* (Oxford Scholarship Online, 2012).
- ⁴⁹R. P. Wang, G. Xu, and P. Jin, Phys. Rev. B **69**(11), 113303 (2004).